Global and Local Regulation of Clathrin-Coated Pit Dynamics Detected on Patterned Substrates

Allen P. Liu, Dinah Loerke, Sandra L. Schmid,* and Gaudenz Danuser*
Department of Cell Biology, Scripps Research Institute, La Jolla, California

ABSTRACT Live-cell imaging of individual clathrin-coated pit (CCP) dynamics has revealed a broad variation in their internalization kinetics, but the functional significance and mechanistic underpinnings of this heterogeneity remain unknown. One contributing factor may be the spatial variations in the underlying actin cortex. To test this, we cultured cells on fibronectin (Fn) micropatterned substrates to vary the cortical actin mechanics in a defined manner. Under these conditions, stress fibers became organized to bridge adhesive islands, creating spatial heterogeneity in the cortical actin architecture. CCP lifetimes within the Fn-coated islands were selectively prolonged. This differential effect was not due to adherence to Fn-coated surfaces, and was not observed in cells grown on patterned surfaces that did not induce organized stress fiber assembly. Pharmacological agents that lower cortical tension selectively lowered CCP lifetimes within Fn islands, thus abolishing the spatial heterogeneity in the CCP dynamics. Although we cannot rule out the possibility that other factors might locally affect CCP dynamics at Fn islands, our data suggest that localized modulation in cortical tension may spatially regulate clathrin-mediated endocytosis.

INTRODUCTION

Clathrin-mediated endocytosis (CME) is initiated by the assembly of coat proteins that, together with other accessory proteins, recruit cargo molecules and drive membrane invagination. Subsequently, dynamin catalyzes fission at the neck of deeply invaginated clathrin-coated pits (CCPs), after which the clathrin-coated vesicles (CCVs) are quickly uncoated and the released proteins are reused in subsequent cycles of CME (1).

Live-cell imaging has revealed broad heterogeneity in the lifetimes, mobility, intensity, and spatial distribution of CCPs (2–4). Based on automated lifetime analysis, a recent study identified three kinetically distinct subpopulations (two abortive and one productive) of CCPs (5). Thus, not every individually observed CCP follows the prescribed life cycle; rather, a significant proportion is aborted, suggesting early regulation of CME efficiency. In addition, the lifetime distribution of the productive CCP population is very broad, ranging from 20 to >90 s. Therefore, it seems very likely that multiple factors contribute to the regulation of maturation efficiency and kinetics of CCV formation.

One such factor could be the local turnover of actin filaments during CCP maturation (6). The plasma membrane and its associated cortical actin network act as a functional unit in many cellular processes, including endocytosis (7). Although actin assembly and disassembly are tightly coupled to endocytosis in yeast (8), the functional significance of actin dynamics is less clear in mammalian cells. Biochemical analyses have revealed a variable role for actin in CME (9), and live-cell imaging has shown that CCV internalization is accompanied by actin polymerization (10,11). Subsequent studies have shown that actin functions at multiple stages of CME (12). The apparent discrepancies in these findings may reflect stochastic and/or spatiotemporally organized variation in actin dynamics that could affect local heterogeneity in CCP dynamics. It is also possible that the structural organization of cortical actin has a more global influence on CME, which has not been previously examined. Such global variation could be an important factor in modulating CME efficiency between different tissues, as well as within tissue and throughout cells.

To investigate the contributions of cortical actin mechanics on the local and global dynamic behavior of CCPs, we used microcontact printing (μCP) to create spatially patterned adhesive and nonadhesive regions on cell substrates. By restricting where cells make focal adhesions (FAs) to extracellular matrix (ECM), μCP provides an effective way to alter cortical actin organization in a spatially defined manner (13,14). We then used total internal reflection fluorescence microscopy (TIR-FM) and computational image analysis to assess the spatial heterogeneity of CCP dynamics on the patterned surfaces.

MATERIALS AND METHODS

Cell culture and reagents

BSC1 monkey kidney epithelial cells stably expressing rat brain EGFP-clathrin light chain (EGFP-LCa) were provided by Dr. T. Kirchhausen (Harvard Medical School, Boston, MA) and cultured as previously described (2). Latrunculin A (latA), and polylysine (PLL), and aminopropyl-triethoxysilane were obtained from Sigma (St. Louis, MO), Y-27632 and ML-7 were purchased from Calbiochem (San Diego, CA), and fibronectin (Fn) was obtained from BD Bioscience (San Jose, CA). PLL-polyethylene glycol (PLL-PEG) was obtained from Surface Solutions (Zurich, Switzerland). PLL-PEG and PLL were labeled with Texas Red succinimidyl ester (Invitrogen, Carlsbad, CA) according to the standard protocol.

Submitted February 19, 2009, and accepted for publication June 3, 2009.

*Correspondence: slschmid@scripps.edu or gdanuser@scripps.edu

Editor: Michael Edidin.

0006-3495/09/08/1038/10 $2.00

doi: 10.1016/j.bpj.2009.06.003

Microcontact printing

Standard soft lithography techniques were used to create the silicon master from which poly-dimethoxy-siloxane (PDMS) stamps were made. To prepare the PDMS stamps, Sylgard-184 elastomer and curing agents (Dow Corning, Midland, MI) were mixed at a ratio of 10:1 and then cast over the mold and cured at 60°C overnight. Inking solution was placed on the PDMS stamps and incubated for 30 min at room temperature. Subsequently, the inking solution was aspirated and the stamps were blown dry with a stream of nitrogen gas before they were placed in conformal contact with a glutaraldehyde-treated coverslip. Glutaraldehyde-functionalized coverslips were made by sequential treatment with 1% aminopropyl-triethoxysilane in ethanol and 6% glutaraldehyde solution in phosphate-buffered saline. For Fn patterns, the inking solution consisted of 40 μg/mL Fn and 20 μg/mL of Alexa fluor 568 fibrinogen (Invitrogen) for visualization. After the stamping was completed, the Fn-patterned substrate was backfilled with 1 mg/mL PLL-PEG for 30 min. For PLL-PEG and PLL patterns, 40 μg/mL Texas Red PLL-PEG or 40 μg/mL Texas Red PLL were added to the stamp. The PLL-PEG-patterned substrate was not backfilled and all patterns were kept in phosphate-buffered saline at 4°C and used within 3 days.

Fluorescence microscopy

TIR-FM was performed exactly as previously described (12). Cells were plated on patterned substrates for at least 2 h before they were imaged in an in-house-made imaging chamber consisting of the patterned coverslip mounted on a slide with two strips of double-sided tape as the spacer. The imaging chamber was filled with Dulbecco's modified Eagle's medium supplemented with 2.5% fetal bovine serum and 20 mM HEPES, and sealed with VALAP (1:1:1 of Vaseline, lanolin, and paraffin). Movies of EGFP-LCa and the pattern were taken at 2 s intervals for 10 min at 37°C. For fluorescent labeling, cells were fixed in 2% glutaraldehye and 0.5% Triton for 2 min followed by another 30 min in 4% glutaraldehyde. Actin filaments were stained using fluorescent phalloidin (Invitrogen), and FAs were detected using mouse anti-paxillin antibody (BD Transduction Laboratory). Fixed samples were imaged on a Nikon TE2000 with a spinning disk confocal module (Perkin Elmer, Waltham, MA) or an Olympus IX71 inverted fluorescence microscope.

Data and image analysis

Custom-written software for single-particle tracking was used to compute trajectories from the complete inventories of CCPs imaged in live-cell microscopy (15). The tracking incorporated a gap-closing scheme that followed unstable signals from CCPs that either contained low amounts of EGFP-LCa or temporarily moved out of the narrow evanescent field of the TIR-FM. We used image segmentation to identify CCPs inside and outside patterned surfaces. In control experiments, we imposed a "mock" pattern on cells grown on a uniform surface, and, as expected, found no difference in the kinetics inside and outside the segmented regions (data not shown). The survival functions were calculated from the lifetime histograms of all CCPs and normalized to the total number of trajectories. We performed Student's *t*-test to calculate the significant *p*-values between different conditions. All images were handled in Photoshop, and any contrast adjustments were applied uniformly to the entire image.

RESULTS

Spatial organization of CCPs, integrin, paxillin, and actin on microfabricated Fn substrates

We used Fn, which binds to and activates integrins, as a model ECM protein, and μCP to geometrically confine ECM binding in regular patterns of adhesive and nonadhesive regions to modulate cortical structure (Fig. 1 *A*). The pattern geometry was chosen based on two criteria: 1), the spacing between ECM-coated regions must enable cells to spread over adhesive and nonadhesive zones; and 2), the adhesive regions must be large enough so that a sufficient number of CCPs can be found within the patterns for statistical analysis. We determined that patterns of 5 μm diameter circles, which encompass ~5–10 CCPs per circular region, spaced 5 or 10 μm apart fulfilled these criteria optimally for our BSC1 cell model (2). A cell spread on this design typically has ~15–20% of the surface area on patterned regions. Fn was covalently attached to the substrate (see Materials and Methods) to prevent cells from internalizing and remodeling the ECM (16). Fn immobilization did not interfere with μCP or CCP lifetime measurements. Once the pattern was transferred, the remaining glass surface was passivated with a block-copolymer PLL-PEG to render it inert to the deposition of serum ECM proteins and those produced by the cells (17).

Staining for $\alpha v\beta 3$ integrins that bind to Fn revealed that they were localized around the periphery of the Fn islands and that CCPs were detected both within and outside the Fn islands (Fig. 1 *B*; see Fig. S1 in the Supporting Material). Mature FAs (detected by strong immunolabeling of the FA protein, paxillin) were also found at the Fn islands, where they mostly accumulated around the periphery. Mature FAs were largely absent from the nonadhesive PLL-PEG areas at the cell periphery (Fig. 1 *C* and Fig. S1). We found that ~80% of the CCPs on Fn islands did not colocalize with the FAs (Fig. S1). Staining of the actin cytoskeleton by fluorescent phalloidin revealed massive bundles of actin filaments (stress fibers) that bridged the Fn islands (Fig. 1 *D*), anchoring at FAs around their peripheries. The restriction of FAs to Fn islands and bridging stress fibers that terminate at FAs are characteristic phenotypes of cells on micropatterned adhesive substrates (18).

CCP lifetimes are prolonged within Fn islands

BSC1 cells stably expressing EGFP-LCa were imaged by TIR-FM at 2 s intervals for 10 min (see Materials and Methods, Movie S1). This acquisition setting captures the heterogeneous dynamics of productive CCPs whose lifetimes range from 20 to >90 s (5). To compute the lifetimes, trajectories of individual CCPs were detected (Fig. 1 *E*) and tracked from their appearance to their disappearance (15). Using image segmentation of the pattern, each CCP was assigned over their lifetimes as being inside or outside the Fn islands (Fig. 1 *F*). CCP densities were homogeneous throughout the patterned substrate; thus, ~15–20% of CCPs were found inside the Fn islands. CCP lifetimes were assembled in a survival function in which the fraction of remaining CCPs was plotted against lifetime. The survival function was shifted toward longer lifetimes for CCPs inside the Fn islands compared to those outside ($n_{cell} = 26, n_{traj} = 85{,}296$; Fig. 1 *G*). Lifetimes at 10% survival fraction were used to calculate the statistical significance of these differences and to compare

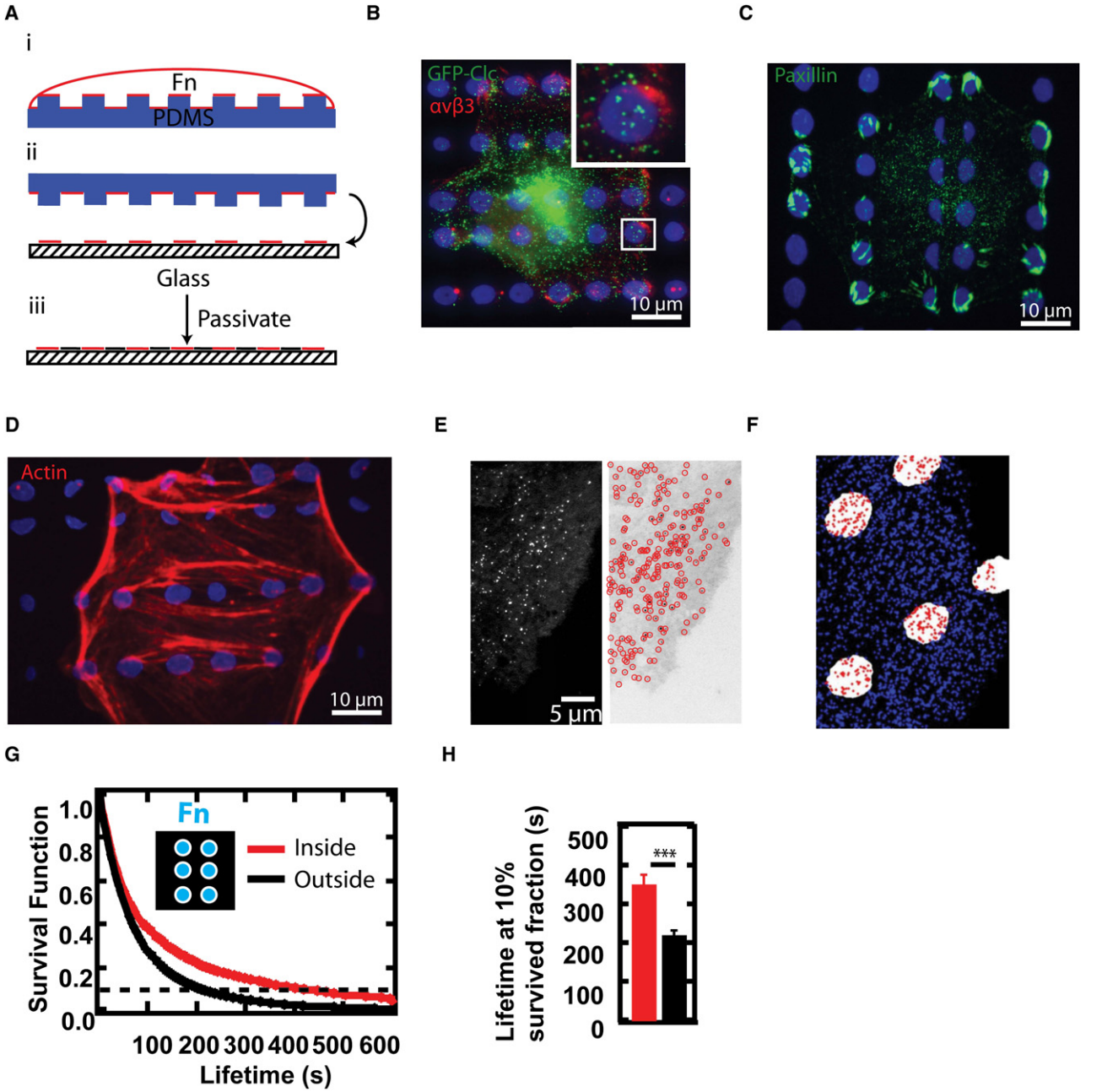

FIGURE 1 Spatial heterogeneity of CCP dynamics on Fn-patterned surfaces. (*A*) Schematics of μCP printing. An elastomeric PDMS stamp is inked with Fn and the Fn is transferred to the glass substrate by conformal contact. The unstamped region is passivated with PLL-PEG. (*B*) BSC1 EGFP-LCa (*green*) cells attached to Fn-patterned substrate (*blue*) are labeled with anti-$\alpha v\beta 3$ antibodies (*red*). (*C* and *D*) BSC1 EGFP-LCa cells attached to Fn-patterned substrate (*blue*) are labeled with anti-paxillin antibodies to localize FAs (*green*, panel *C*) or with fluorescent phalloidin to label actin filaments (*red*, panel *D*). (*E*) TIRF image of EGFP-LCa-containing CCPs (*left*). Result of CCP identification by particle detection (*red circles*) overlaid on the inverted image (*right*). (*F*) Segmentation of patterned region and CCP trajectories. Red and blue dots respectively denote trajectories within and outside the patterned regions in white. (*G*) Survival function of CCPs on Fn-patterned substrate showing significantly longer CCP lifetimes inside compared to outside Fn islands. The dotted line is drawn across the 10% survival fraction. (*H*) Lifetime (mean $\pm$ SD) of 10% survived fractions of CCPs inside (*red*) compared to outside (*black*) Fn islands. *** $p < 1 \times 10^{-4}$.

different experimental conditions. The CCP lifetimes at 10% survival fraction were significantly prolonged within the Fn islands (353 $\pm$ 24 s) compared to outside the Fn pattern (222 $\pm$ 13 s; Fig. 1 *H*). As indicated by the offset of the survival function at 600s, ~4.5% of CCPs on Fn islands persisted throughout the entire 10 min movie, compared with ~1.9% of CCPs outside these regions. The prolonged lifetime inside the Fn patterns indicates that a lower initiation density for CCPs results in homogeneous densities throughout the patterned substrate. Indeed, initiation densities were found to be lower inside the patterns compared to outside the patterns (Fig. S2), although the difference was not statistically

significant. The relatively high statistical uncertainty of the initiation density originates in the much fewer data points that can be collected inside the pattern. In summary, these data suggest that the lifetime and initiation of CCPs are affected by the different substrate properties across the micropatterns.

Spatial heterogeneity of CCP lifetimes is not observed on chemically uniform Fn substrates

To examine whether adhesion and/or integrin signaling via FA influences CCP dynamics, we measured CCP lifetimes on chemically uniform surfaces coated with increasing concentrations of covalently immobilized Fn, yielding increased activation of integrin-mediated signaling (19). The organization of FAs and actin filaments on these chemically uniform substrates did not resemble those on Fn-patterned substrates (40 μg/mL Fn; Fig. 2 *A*). The FAs were not spatially restricted, and stress fibers were less pronounced and appeared randomly distributed. In contrast to the reduced rate of CCV formation on Fn islands, uniformly increasing Fn density led to a small, statistically insignificant decrease of lifetime in the survival functions (Fig. 2 *B*). Thus, adhesion per se, including the possibility of frustrated CME of Fn receptors, cannot account for the differential CCP lifetimes observed within the Fn islands.

Global increase in CCP lifetimes on Fn-patterned substrates

Unexpectedly, the lifetimes of CCPs budding from the uniformly adherent Fn substrate were significantly shorter than those budding from even the nonadherent surfaces outside the Fn patterned substrate (145 $\pm$ 7 s vs. 222 $\pm$ 13 s 10% survival time; compare *black bars* in Figs. 2 *B* and 1 *H*, respectively). This further argues that adherence alone does not limit the rate of CCV formation. CCPs have been shown in some cells to interact with and align along stress fibers, which could account for the slower kinetics of internalization between Fn islands (20). However, we did not detect alignment of long-lived CCPs in nonadherent regions, as would be expected if they were associated with the stress fibers that span these regions (Fig. S3). Together, these data suggest that, in addition to the localized heterogeneity of CCP dynamics observed inside and outside the Fn islands, the adherence of cells on Fn-patterned surfaces also exerts a global effect on CCP dynamics.

Spatial heterogeneity of CCP lifetimes is not observed on PLL-PEG or PLL patterns

Next we investigated CCP lifetimes on other patterned substrates. First, cells were plated on inverted patterns in which PLL-PEG was stamped instead of Fn with no passivation. This yielded ~80–85% of the cell area on adhesive regions, compared with ~15–20% for Fn-patterned substrates.

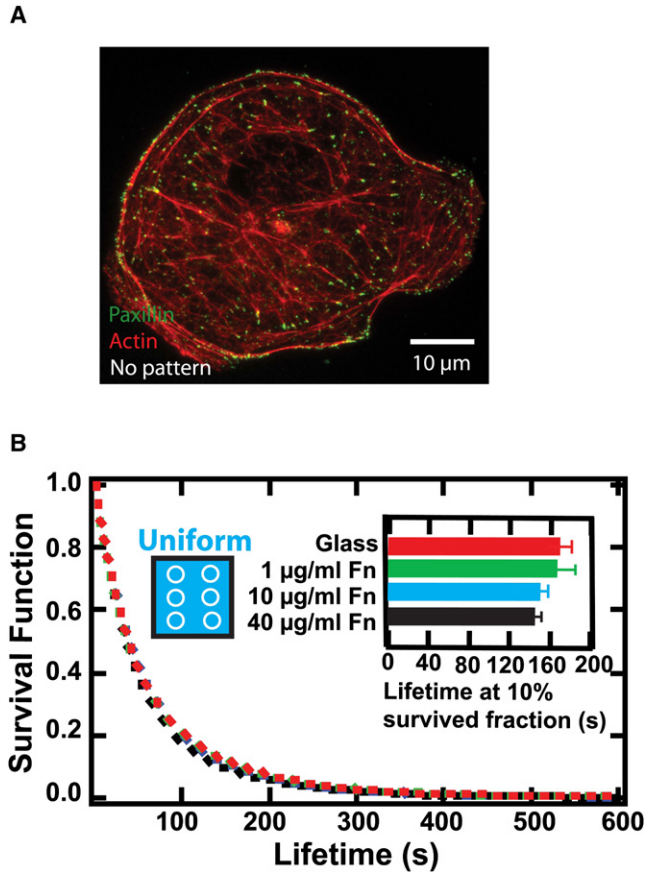

FIGURE 2 CCP lifetimes are not significantly affected by the Fn density of uniformly coated surfaces. (*A*) Fluorescence micrograph of paxillin and actin in a BSC1 cell plated on uniform 40 μg/mL Fn substrates. FAs and actin filaments were stained with anti-paxillin antibody and AF568 phalloidin, respectively. (*B*) Survival functions of CCPs on untreated coverslips compared to coverslips uniformly coated with different concentrations of Fn. The 10% survived fraction is summarized in the inset (mean $\pm$ SD). The differences in CCP lifetimes for cells plated on uniform surfaces are not significant ($p > 0.05$).

As expected, FAs failed to assemble on the PLL-PEG islands, and actin filaments formed a radial pattern uniformly distributed throughout the cell (Fig. 3 *A*). The difference between this organization of actin filaments and that seen in cells plated on Fn patterns reflects the fact that stress fibers are required to bridge the longer distances between adhesive islands on Fn patterns to maintain cell shape, whereas for the inverted patterns, the intrinsic tension of the cortex is sufficient to maintain mechanical integrity (21,22). On the PLL-PEG-patterned surface, CCP lifetime distributions were identical between adhesive and nonadhesive regions ($n_{cell} = 8$; $n_{traj} = 55{,}983$; Fig. 3 *B*). Their lifetimes at a 10% survival fraction were also identical to those on a uniform Fn surface (Fig. 3 *E*). Thus, neither the observed spatial heterogeneity of CCP dynamics nor the global increase in CCP lifetimes observed on Fn patterns can be explained simply by cells responding to a spatially nonuniform chemical surface.

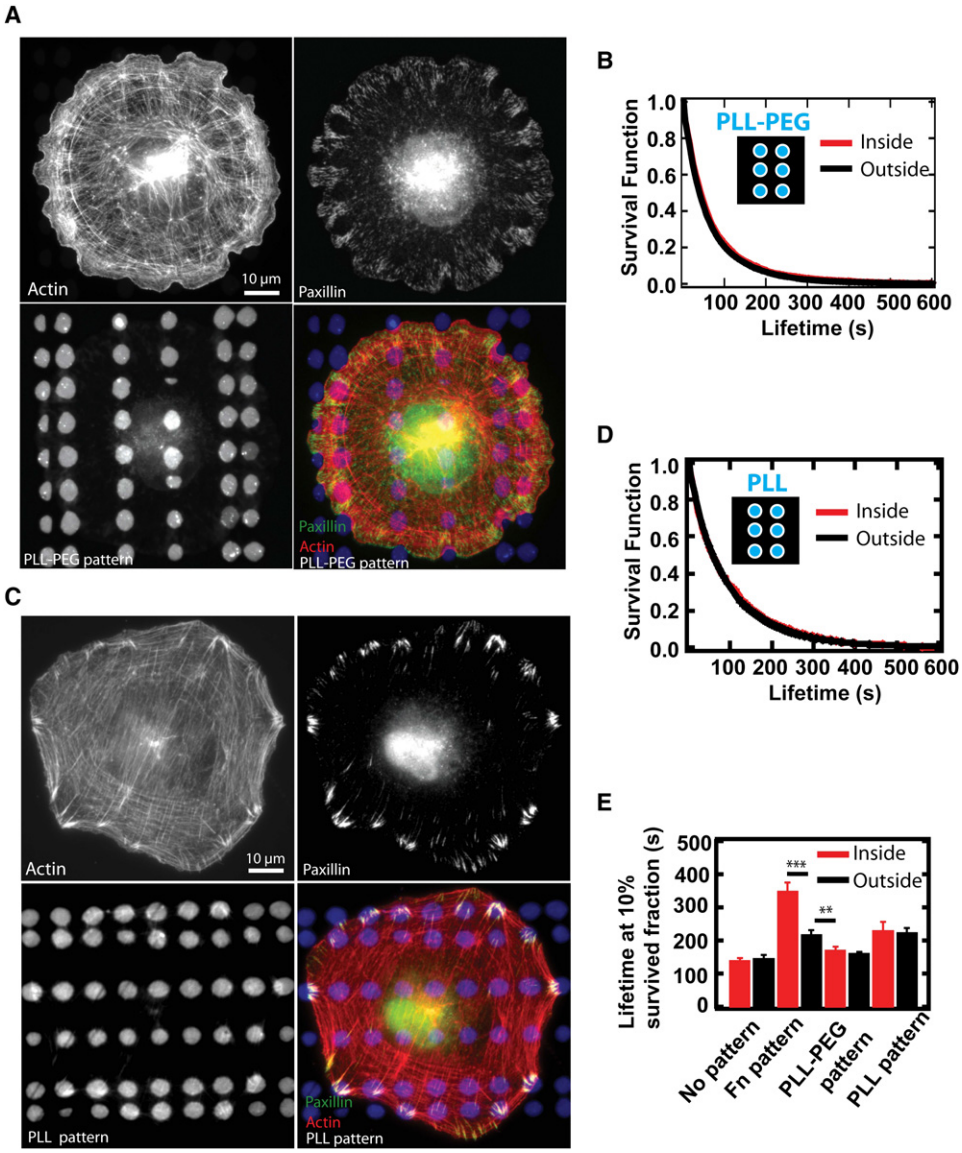

FIGURE 3 Spatial heterogeneity of CCP dynamics is abolished on PLL-PEG and PLL patterned surfaces. (*A*) Fluorescence micrographs of actin and paxillin in BSC1 cells plated on PLL-PEG patterns. (*B*) Survival function of CCPs on PLL-PEG patterns. (*C*) Fluorescence micrographs of actin and paxillin in BSC1 cells plated on PLL patterns. (*D*) Survival function of CCPs on PLL patterns. (*E*) Summary of lifetimes of 10% survived fractions for different micropatterns (mean ± SD). ** $p < 0.01$; *** $p < 1 \times 10^{-4}$.

By inverting the patterns, we altered the ratio of adhesive to nonadhesive areas. Thus, it remained possible that the observed spatial heterogeneity in lifetime was due to the molecular crowding of adhesion to small areas. To test this, we plated cells on patterned PLL substrates, where cells are able to adhere, but adhesion does not activate integrins (17). Indeed, the cortical organization was mostly uniform throughout the cell, although some stress fibers were observed to emanate from and bridge adjacent to PLL islands (Fig. 3 *C*). There was no spatial difference in CCP survival functions ($n_{cell} = 13$; $n_{traj} = 73{,}620$; Fig. 3 *D*); however, the 10% survival lifetime for CCPs on the PLL pattern was longer than on unpatterned and PLL-PEG-patterned substrates, and it was comparable to the lifetime on the nonadherent areas on Fn-patterned surfaces (Fig. 3 *E*). Thus, a global increase in CCP lifetimes was observed in both cases in which a smaller area of the cells was adherent. This global effect on CCP lifetimes may be related to increased stress fiber formation across nonadherent regions in these cells, which is known to correlate with increased cytoskeleton tension (23). Alternatively, it may reflect the differential chemical environment in nonadherent regions due to passivation by PLL-PEG.

Pharmacological agents that reduce cortical tension abolish the spatial heterogeneity of CCP lifetimes on Fn-patterned substrates

Only cells plated on Fn-patterned substrates exhibited spatial heterogeneity in CCP lifetimes. This localized effect on CCP dynamics correlated with the unique spatial organization of FAs and actin stress fibers obtained on these patterns. To further explore the mechanisms that might account for this spatial heterogeneity, we next examined the contribution of

cortical actin organization. Cortical actin networks have been established as the primary source of local cortical tension, and depolymerization of the actin cytoskeleton is known to decrease cortical tension (24). In addition, contractility of the actomyosin cortex is responsible for the maintenance of cortical tension (25). Thus, to acutely reduce cortical tension, we applied low doses of pharmacological agents that target cortical actin assembly and contractility.

Previous studies that investigated the roles of actin in endocytosis (9,12,26) used concentrations of latA in the range of 1–5 μM. At these high concentrations, the integrity of the actin cytoskeleton and signaling is severely compromised (27). We found that with 25 nM latA, cells maintained their morphology and the dynamics of the CCPs could be stably monitored by TIR-FM. Under these conditions, neither the localization of paxillin on Fn islands nor the stress fibers between Fn islands appeared to be significantly affected, whereas at 50 nM latA, >90% of cells rounded up within 30 min (Fig. 4 *A*). Nonetheless, treatment of BSC1 cells with 25 nM latA resulted in a detectable shift of actin from Triton-X 100 insoluble (F-actin) fractions to monomeric G-actin (Fig. 4 *B*). The contribution of F-actin decreased from 62.4% to 41.4% of total actin after latA treatment, presumably leading to reduced filament density mainly in cortical networks, as the more compact stress fibers were less affected. Addition of latA to cells on Fn-patterned substrates decreased the lifetime of CCPs within adhesive regions and abolished the spatial heterogeneity of CCP lifetimes ($n_{cell} = 10$; $n_{traj} = 47{,}180$; Fig. 4, *C* and *F*). The lifetimes outside the patterned regions were unaffected, indicating that these low concentrations of latA had no global effect on CCP lifetimes (Fig. 4 *F*). The spatially restricted increase in the rate of CCV formation at Fn islands after treatment with 25 nM latA could be a consequence of either a relief of local cortical actin tension in adhesive regions or a relaxation of a physical barrier created by cortical actin and/or FA contacts that could impede CCP internalization.

An alternative mechanism for regulating cortical tension without affecting the density of actin filaments is myosin-dependent contractility. Myosin activity is controlled by Rho kinase and myosin light-chain kinase (28). The myosin light-chain kinase inhibitor ML-7 (2 μM) and Rho kinase inhibitor Y-27632 (3 μM) were used to acutely reduce the activity of both pathways and thus reduce overall myosin contraction. This perturbation did not alter the localization and distribution of paxillin on the Fn islands or the actin stress fibers that bridged the Fn islands (Fig. 4 *D*). However, inhibition of contractility specifically decreased CCP lifetimes inside the Fn islands, again alleviating the spatial heterogeneity in CCP lifetime distribution inside and outside the patterns ($n_{cell} = 6$; $n_{traj} = 40{,}780$; Fig. 4, *E* and *F*). This result argues against the notion that a physical barrier to CCV formation plays the predominant role in prolonging lifetimes on Fn islands. Together with the latA effects, these data suggest that high, localized cortical tension at the Fn islands imposed by peripherally anchored actin stress fibers reduces the rate of CCV formation. Relaxation of this localized cortical tension either by cortical actin disassembly or by reduced myosin II contractility enhances CME efficiency.

Global changes in the diffusion coefficient and confinement radius of CCPs

The lifetime distribution outside Fn patterns remained the same before and after drug treatments (Fig. 4 *F*), indicating that the effects of these drugs on the kinetics of CCV formation are local and not global. This was somewhat unexpected, given that the actin cortex and actomyosin network extend throughout the cell. The restricted effects provide additional evidence that regions of locally high cortical tension across the Fn islands are especially sensitive to these mild drug treatments. However, given that CCP dynamics are slower even on nonadherent regions of Fn-patterned surfaces relative to uniform surfaces, we sought further evidence for more global effects of cortical tension on CCP dynamics. Previous studies suggested that the actin cortex might globally limit the lateral mobility of CCPs (3); therefore, we investigated other dynamic aspects of CCP behavior that might be more sensitive indicators of the global effects of these drugs on cortical tension.

Two independent kinematic parameters of CCP mobility, the diffusion coefficient and confinement radius, can be readily computed from CCP trajectories (29) and report the behavior of two different classes of CCPs: freely diffusing and confined. In contrast to the spatial heterogeneity of CCP lifetimes, we found no difference in the mobility of CCPs inside or outside the Fn islands (Fig. S4), suggesting a threshold effect of cortical tension on these parameters, and further supporting the notion that CCPs inside Fn islands are not constrained by molecular crowding. However, consistent with a higher global cortical tension, the diffusion coefficients for CCPs on Fn patterns were significantly lower than those in cells cultured on uniform surfaces (Fig. 5 *A*, *light gray* and *black bars*). As expected, LatA and ML-7/Y-27632 treatments, which decrease cortical tension, increased the diffusion coefficients of CCPs in cells cultured on Fn patterns (Fig. 5 *A*, *dark gray* and *black bars*). A similar pattern of results was obtained when confinement radii were measured (Fig. 5 *B*). Together these findings strengthen our conclusion that cells cultured on Fn patterns exhibit higher global cortical tension, resulting in overall increased CCP lifetimes and reduced lateral mobility.

DISCUSSION

Microcontact printing has been used extensively to probe the effects of cytoskeletal tension on cell shape, but few studies have reported localized changes in a cellular function in response to such conditions. We have shown that spatial heterogeneity in CCP lifetimes can be induced on

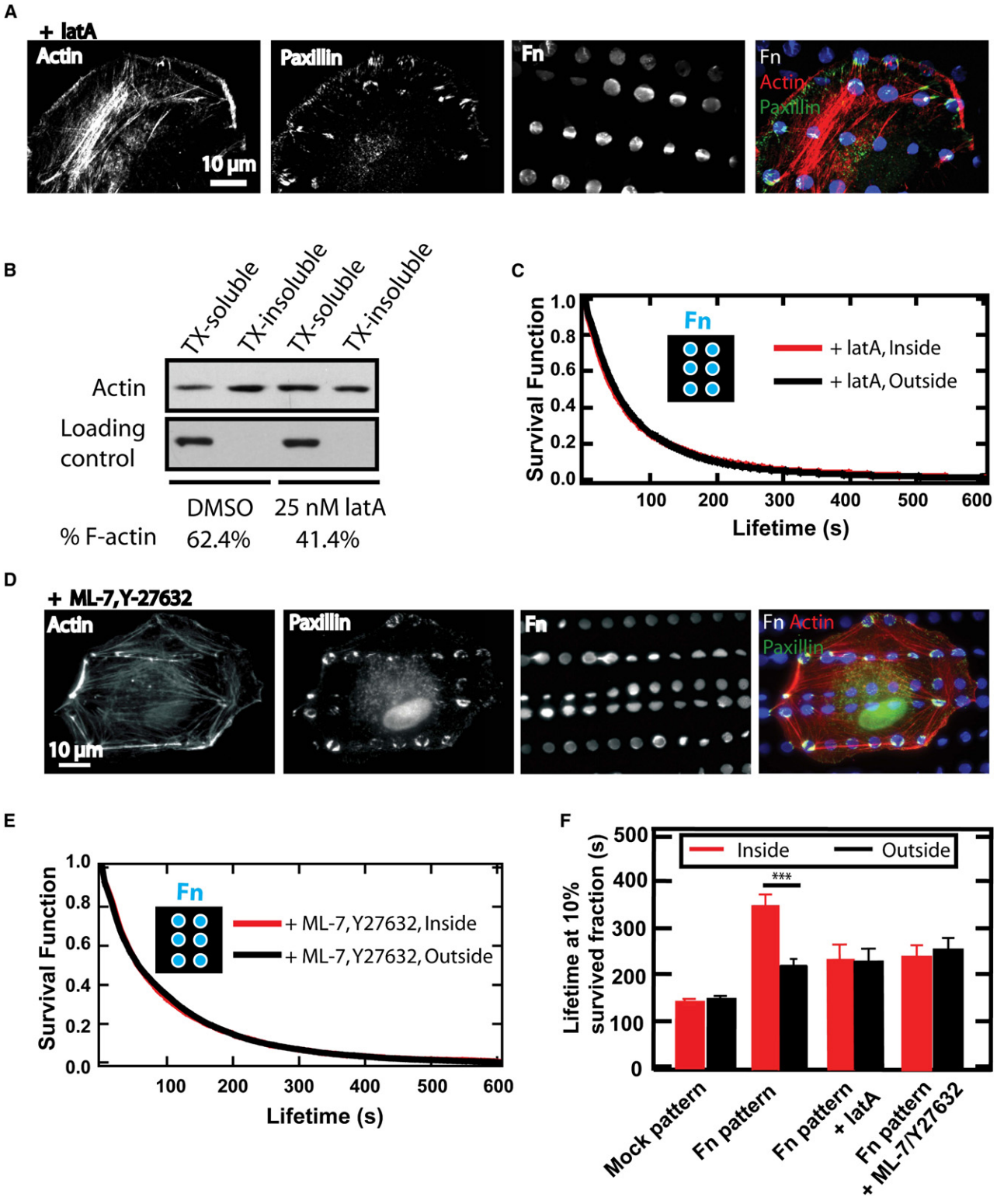

FIGURE 4 Spatial heterogeneity of CCP dynamics is abolished after latA and ML-7/Y27632 drug treatments. (*A*) Fluorescence micrographs of actin and paxillin in BSC1 cells plated on Fn patterns after treatment with 25 nM latA. (*B*) Biochemical characterization of shift in F- to G-actin equilibrium after treatment with 25 nM latA. (*C*) Survival function of CCPs on Fn patterns after latA treatment shows no spatial heterogeneity of CCP lifetime. (*D*) Fluorescence micrographs of actin and paxillin in BSC1 cells plated on Fn patterns and treated with 2 μM ML-7 and 3 μM Y-27632. (*E*) Survival function of CCPs on Fn patterns with ML-7/Y27632 treatment shows no spatial heterogeneity of CCP lifetime. (*F*) Summary of lifetimes of 10% survived fractions for different micropatterns (mean $\pm$ SD). *** $p < 1 \times 10^{-4}$.

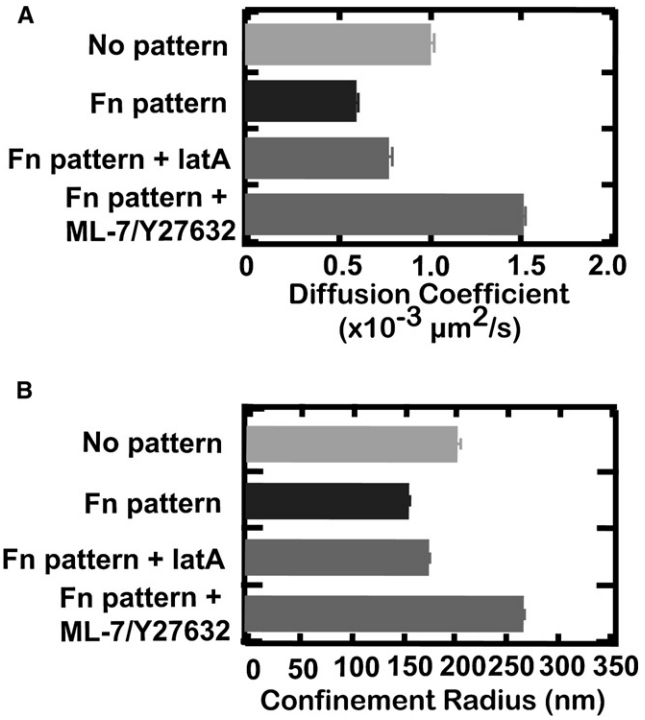

FIGURE 5 Kinematic behaviors of CCPs are globally affected under different conditions. (*A*) Diffusion coefficient of freely diffusing CCPs from five cells on uniform or Fn-patterned surfaces and after the indicated drug treatment (average ± SE). (*B*) Confinement radius of confined CCPs from five cells on different patterned surfaces and after indicated drug treatment (average ± SE). Gray bar shows uniform surface. Black bar shows Fn pattern data. Dark gray bars show drug perturbation data. See Fig. S4 *B* for the number of CCPs used for mobility measurements.

microfabricated Fn substrates. We further showed that this effect is dependent on a contractile and intact cytoskeleton that forms stress fibers across Fn islands unique to the micropatterned substrates used in this study. Using microfabricated beams that acted as force sensors, Tan et al. (23) showed that stress fiber formation at Fn sites correlates with increasing cytoskeletal tension. On micropatterned substrates, traction forces are transmitted at FAs to the nearby cortical actin network via actin stress fibers (21). Thus, we speculate that the increase in localized cortical tension across Fn islands is the primary factor contributing to the decrease in CME efficiency and the kinetics of CCV formation.

Although we favor the localized effect of cortical tension, we cannot completely exclude the possibility that other factors might selectively reduce the rate of CCV formation within Fn islands. For example, it is possible that interactions between Fn receptors (i.e., integrins) and the immobilized Fn could create ''frustrated endocytosis'' and thus slow CCV formation. Indeed, Chetrit et al. (30) recently showed that Dab2, a monomeric adaptor protein, associates with activated integrin molecules to form long-lived Dab2-clathrin platforms. However, the following evidence suggests that this does not apply to our experiments: $\alpha_v\beta_3$ integrins that bind to Fn were found to localize mostly at the periphery of Fn islands, and did not colocalize with CCPs that were found within the islands (Fig. 1 and Fig. S1). Moreover, Fn was also covalently linked to the coverslips when a uniform substrate was formed, but there was no decrease in the rate of CCP internalization (Fig. 2). Instead, we believe that CME could be regulated by the local molecular environment at the Fn islands.

Integrin clustering and activation trigger a cascade of phosphorylation events, and it is also possible that localized signaling from surrounding integrins and FAs can either directly or indirectly affect CCP dynamics. The primary function of integrin signaling is to promote engagement of stress fibers with FAs and to stimulate dendritic actin network assembly (31,32). The stress fibers and the dendritic cortical actin network are mechanically coupled via various actin-binding proteins (e.g., myosin and α-actinin (33)) and are expected to generate locally high cortical tension through actomyosin contractility. Our observation that inhibition of actomyosin contractility abolishes the spatial heterogeneity is consistent with the interpretation that integrin-induced increases in cortical tension at and near the adhesion zone are primarily responsible for the reduced rates of CCV formation. Of importance, even though stress fiber formation is observed in cells plated on PLL patterns, there is no spatial heterogeneity of CCP dynamics in the adherent zones, indicating that integrin signaling plays an important role in establishing the unique properties of Fn-island microdomains.

The most likely alternative factor affecting localized CCP dynamics is the molecular crowding that can arise from the discrete localization of FA proteins and subsequent crowding of stress fibers and associated proteins at these FAs. In our experimental setup, it is impossible to completely uncouple the spatially restricted organization of FAs and stress fiber assembly from cortical tension, as the latter is dependent on the former. Therefore, we cannot rule out this alternate interpretation of our findings. Nonetheless, the following observations argue against this interpretation: 1), 80% of CCPs within Fn islands do not colocalize with FAs (Fig. S1); 2), there is little difference in the initiation density of CCPs within and outside Fn islands (Fig. S2); 3), longer-lived CCPs are heterogeneously distributed within Fn islands (Fig. S3); and 4), there is no spatial heterogeneity in the diffusion coefficients of CCPs within or outside the Fn islands (Fig. S4). Moreover, inhibitors of myosin II contractility, which are not expected to alter the localized concentration of FA and stress fibers, abrogate the differential kinetics of CCV formation inside the Fn islands. Thus, we favor the hypothesis that high localized cortical tension at Fn-islands slows CME within these regions.

In addition to localized integrin signaling and areas of high cortical tension at adherent islands, stress fibers that form when cells are grown on patterned substrates are known to generate cellular prestress (34). Consistent with this, we observed a general decrease in the rate of CCV formation

in nonadherent regions only when cells were cultured on patterned surfaces that induce the formation of stress fibers (i.e., Fn and PLL patterns). It is difficult to conceive how a crowding mechanism could lead to globally elevated lifetimes on patterned substrates. Although the rate of CCV formation in nonadherent regions was not restored by treatment with latA or myosin inhibitors, we did see global effects on other aspects of CCP kinematics. This suggests a threshold in sensitivity to the local variations in CCV formation kinetics immediately adjacent to FAs. Other methods will be needed to more directly vary and measure the effects of cortical tension on CCP dynamics.

In summary, our results show that local variations in cortical mechanics can spatially regulate CCP dynamics and thus contribute to the functional heterogeneity of CCPs. It is important to point out that cortical tension is different from membrane tension. The observation that the addition of amphiphilic compounds to mitotic cells increases the rate of fluid-phase uptake has led to the suggestion that membrane tension is an important physical regulator of endocytosis (35). Cortical tension derives from the interactions of the underlying cortical actin network with the plasma membrane. The observed spatial variations in CME efficiency as a result of spatial variations in cortex organization are likely to be physiologically relevant. In tissues, ECM architecture ranges from a homogeneous meshwork to a fibrillar scaffold (36,37). The cytoskeleton responds to the adhesive microenvironment accordingly. Our observations demonstrate that these mechanical and/or chemical inputs can significantly modulate CME.

These experiments establish a link between the mechanical state of a cell and its receptor homeostasis. Clearly, such a relation may be of fundamental importance to many physiological and pathophysiological functions. For example, sharp and temporally variable spatial differences in cortical tension are known to occur during cell morphogenic events such as migration (38) and division (39), and processes such as apoptosis and differentiation have been directly related to micromechanical environments (40,41). It was recently shown that local cortical tension guides endothelial cell branching in three dimensions (42). Similarly, major force gradients across tissues undergoing morphogenesis have been observed (43), and normal and cancerous cells are known to have significantly different mechanical properties (44). It is tempting to speculate that, in these contexts, resultant variations in CME efficiency may be one of the mechanisms that convert mechanical inputs into spatially controlled signals.

SUPPORTING MATERIAL

Four figures and a movie are available at http://www.biophysj.org/biophysj/supplemental/S0006-3495(09)01053-4.

We thank the BioMEMS Resource Center (Charlestown, MA) and Daniel Irimia for fabricating the silicon master used to make the PDMS stamps, James Lim for designing the photo-mask, Ian Schneider and members of the Schmid and Danuser laboratories for helpful comments, and Carlos Barbas for providing the anti-$\alpha_v\beta_3$ antibodies.

This work was supported by the National Institutes of Health (grant GM73165 to G.D. and S.L.S.).

REFERENCES

1. Conner, S. D., and S. L. Schmid. 2003. Regulated portals of entry into the cell. *Nature*. 422:37–44.
2. Ehrlich, M., W. Boll, A. Van Oijen, R. Hariharan, K. Chandran, et al. 2004. Endocytosis by random initiation and stabilization of clathrin-coated pits. *Cell*. 118:591–605.
3. Gaidarov, I., F. Santini, R. A. Warren, and J. H. Keen. 1999. Spatial control of coated-pit dynamics in living cells. *Nat. Cell Biol.* 1:1–7.
4. Rappoport, J. Z., B. W. Taha, and S. M. Simon. 2003. Movement of plasma-membrane-associated clathrin spots along the microtubule cytoskeleton. *Traffic*. 4:460–467.
5. Loerke, D., M. Mettlen, D. Yarar, K. Jaqaman, H. Jaqaman, G. Danuser, and S. L. Schmid. 2009. Cargo and dynamin regulate clathrin-coated pit maturation. *PLos Biol.* 7:0628–0639.
6. Qualmann, B., M. M. Kessels, and R. B. Kelly. 2000. Molecular links between endocytosis and the actin cytoskeleton. *J. Cell Biol.* 150:F111–F116.
7. Doherty, G. J., and H. T. McMahon. 2008. Mediation, modulation, and consequences of membrane-cytoskeleton interactions. *Annu. Rev. Biophys.* 37:65–95.
8. Engqvist-Goldstein, A. E., and D. G. Drubin. 2003. Actin assembly and endocytosis: from yeast to mammals. *Annu. Rev. Cell Dev. Biol.* 19:287–332.
9. Fujimoto, L. M., R. Roth, J. E. Heuser, and S. L. Schmid. 2000. Actin assembly plays a variable, but not obligatory role in receptor-mediated endocytosis in mammalian cells. *Traffic*. 1:161–171.
10. Merrifield, C. J., B. Qualmann, M. M. Kessels, and W. Almers. 2004. Neural Wiskott Aldrich syndrome protein (N-WASP) and the Arp2/3 complex are recruited to sites of clathrin-mediated endocytosis in cultured fibroblasts. *Eur. J. Cell Biol.* 83:13–18.
11. Merrifield, C. J., M. E. Feldman, L. Wan, and W. Almers. 2002. Imaging actin and dynamin recruitment during invagination of single clathrin-coated pits. *Nat. Cell Biol.* 4:691–698.
12. Yarar, D., C. M. Waterman-Storer, and S. L. Schmid. 2005. A dynamic actin cytoskeleton functions at multiple stages of clathrin-mediated endocytosis. *Mol. Biol. Cell*. 16:964–975.
13. Bischofs, I. B., F. Klein, D. Lehnert, M. Bastmeyer, and U. S. Schwarz. 2008. Filamentous network mechanics and active contractility determine cell and tissue shape. *Biophys. J.* 95:3488–3496.
14. Thery, M., A. Pepin, E. Dressaire, Y. Chen, and M. Bornens. 2006. Cell distribution of stress fibres in response to the geometry of the adhesive environment. *Cell Motil. Cytoskeleton*. 63:341–355.
15. Jaqaman, K., D. Loerke, M. Mettlen, H. Kuwata, S. Grinstein, et al. 2008. Robust single particle tracking in live cell time-lapse sequences. *Nat. Methods*. 5:695–702.
16. Sottile, J., and J. Chandler. 2005. Fibronectin matrix turnover occurs through a caveolin-1-dependent process. *Mol. Biol. Cell*. 16:757–768.
17. Csucs, G., R. Michel, J. W. Lussi, M. Textor, and G. Danuser. 2003. Microcontact printing of novel co-polymers in combination with proteins for cell-biological applications. *Biomaterials*. 24:1713–1720.
18. Lehnert, D., B. Wehrle-Haller, C. David, U. Weiland, C. Ballestrem, et al. 2004. Cell behaviour on micropatterned substrata: limits of extracellular matrix geometry for spreading and adhesion. *J. Cell Sci.* 117:41–52.
19. Asthagiri, A. R., C. M. Nelson, A. F. Horwitz, and D. A. Lauffenburger. 1999. Quantitative relationship among integrin-ligand binding, adhesion, and signaling via focal adhesion kinase and extracellular signal-regulated kinase 2. *J. Biol. Chem.* 274:27119–27127.

20. Bennett, E. M., C. Y. Chen, A. E. Engqvist-Goldstein, D. G. Drubin, and F. M. Brodsky. 2001. Clathrin hub expression dissociates the actin-binding protein Hip1R from coated pits and disrupts their alignment with the actin cytoskeleton. *Traffic*. 2:851–858.

21. Balaban, N. Q., U. S. Schwarz, D. Riveline, P. Goichberg, G. Tzur, et al. 2001. Force and focal adhesion assembly: a close relationship studied using elastic micropatterned substrates. *Nat. Cell Biol.* 3:466–472.

22. Csucs, G., K. Quirin, and G. Danuser. 2007. Locomotion of fish epidermal keratocytes on spatially selective adhesion patterns. *Cell Motil. Cytoskeleton.* 64:856–867.

23. Tan, J. L., J. Tien, D. M. Pirone, D. S. Gray, K. Bhadriraju, et al. 2003. Cells lying on a bed of microneedles: an approach to isolate mechanical force. *Proc. Natl. Acad. Sci. USA.* 100:1484–1489.

24. Wakatsuki, T., B. Schwab, N. C. Thompson, and E. L. Elson. 2001. Effects of cytochalasin D and latrunculin B on mechanical properties of cells. *J. Cell Sci.* 114:1025–1036.

25. Paluch, E., C. Sykes, J. Prost, and M. Bornens. 2006. Dynamic modes of the cortical actomyosin gel during cell locomotion and division. *Trends Cell Biol.* 16:5–10.

26. Sankaranarayanan, S., P. P. Atluri, and T. A. Ryan. 2003. Actin has a molecular scaffolding, not propulsive, role in presynaptic function. *Nat. Neurosci.* 6:127–135.

27. Na, S., O. Collin, F. Chowdhury, B. Tay, M. Ouyang, et al. 2008. Rapid signal transduction in living cells is a unique feature of mechanotransduction. *Proc. Natl. Acad. Sci. USA.* 105:6626–6631.

28. Matsumura, F., G. Totsukawa, Y. Yamakita, and S. Yamashiro. 2001. Role of myosin light chain phosphorylation in the regulation of cytokinesis. *Cell Struct. Funct.* 26:639–644.

29. Ewers, H., A. E. Smith, I. F. Sbalzarini, H. Lilie, P. Koumoutsakos, et al. 2005. Single-particle tracking of murine polyoma virus-like particles on live cells and artificial membranes. *Proc. Natl. Acad. Sci. USA.* 102:15110–15115.

30. Chetrit, D., N. Ziv, and M. Ehrlich. 2009. Dab2 regulates clathrin assembly and cell spreading. *Biochem. J.* 418:701–715.

31. Vicente-Manzanares, M., C. K. Choi, and A. R. Horwitz. 2009. Integrins in cell migration—the actin connection. *J. Cell Sci.* 122: 199–206.

32. Puklin-Faucher, E., and M. P. Sheetz. 2009. The mechanical integrin cycle. *J. Cell Sci.* 122:179–186.

33. Choi, C. K., M. Vicente-Manzanares, J. Zareno, L. A. Whitmore, A. Mogilner, et al. 2008. Actin and alpha-actinin orchestrate the assembly and maturation of nascent adhesions in a myosin II motor-independent manner. *Nat. Cell Biol.* 10:1039–1050.

34. Kumar, S., I. Z. Maxwell, A. Heisterkamp, T. R. Polte, T. P. Lele, et al. 2006. Viscoelastic retraction of single living stress fibers and its impact on cell shape, cytoskeletal organization, and extracellular matrix mechanics. *Biophys. J.* 90:3762–3773.

35. Raucher, D., and M. P. Sheetz. 1999. Membrane expansion increases endocytosis rate during mitosis. *J. Cell Biol.* 144:497–506.

36. Abrams, G. A., S. L. Goodman, P. F. Nealey, M. Franco, and C. J. Murphy. 2000. Nanoscale topography of the basement membrane underlying the corneal epithelium of the rhesus macaque. *Cell Tissue Res.* 299:39–46.

37. Wezeman, F. H. 1998. Morphological foundations of precartilage development in mesenchyme. *Microsc. Res. Tech.* 43:91–101.

38. Kole, T. P., Y. Tseng, I. Jiang, J. L. Katz, and D. Wirtz. 2005. Intracellular mechanics of migrating fibroblasts. *Mol. Biol. Cell.* 16:328–338.

39. Effler, J. C., Y. S. Kee, J. M. Berk, M. N. Tran, P. A. Iglesias, et al. 2006. Mitosis-specific mechanosensing and contractile-protein redistribution control cell shape. *Curr. Biol.* 16:1962–1967.

40. Ingber, D. E. 2008. Can cancer be reversed by engineering the tumor microenvironment? *Semin. Cancer Biol.* 18:356–364.

41. Engler, A. J., S. Sen, H. L. Sweeney, and D. E. Discher. 2006. Matrix elasticity directs stem cell lineage specification. *Cell.* 126:677–689.

42. Fischer, R. S., M. Gardel, X. Ma, R. S. Adelstein, and C. M. Waterman. 2009. Local cortical tension by myosin II guides 3D endothelial cell branching. *Curr. Biol.* 19:260–265.

43. Martin, A. C., M. Kaschube, and E. F. Wieschaus. 2009. Pulsed contractions of an actin-myosin network drive apical constriction. *Nature*. 457:495–499.

44. Lam, W. A., M. J. Rosenbluth, and D. A. Fletcher. 2008. Increased leukaemia cell stiffness is associated with symptoms of leucostasis in paediatric acute lymphoblastic leukaemia. *Br. J. Haematol.* 142:497–501.